Laser and Particle Beams (2013), *31*, 643–652.

doi:10.1017/S0263034613000633

Application of high speed frame camera on the intense electron beam accelerator: An overview

XIN-BING CHENG, JIN-LIANG LIU, AND BAO-LIANG QIAN

College of Optoelectronic Science and Engineering, National University of Defense Technology, Changsha, Hunan, Peoples Republic of China

(RECEIVED 27 May 2013; ACCEPTED 26 June 2013)

Abstract

High speed framing camera (HSFC) could be used to capture the image of the electron beams generated by the intense electron-beam accelerator (IEBA), and it is useful to visualize the evolution of discharging and plasma generation phenomenon. So an overview of the application of HSFC on the IEBA is presented. First, we introduce the synchronization problem of HSFC and IEBA, and a synchronization trigger system which could provide a trigger signal with rise time of 17 ns and amplitude of about 5 V is presented. Second, an imaging system based on IEBA, HSFC, and the synchronization trigger system is developed, and it can be used to image the developmental process of plasma in the output vacuum chamber of IEBA and to measure the electrical parameter of IEBA and electrical trigger signal in real time. Furthermore, the imaging system is used to investigate the developmental process of the electron beam of the A-K gap in vacuum under 180 nanosecond quasi-square pulses. It is obtained that the short A-K gap is closed prematurely under long pulse operation with plasma expansion velocity of about 6.25 cm/μs and the light emission in the A-K gap region has the characteristics of "re-ignition" with light duration time about 3800 ns. At last, the discharging process of surface flashover channel of poly-methyl methacrylate (PMMA) insulator with gap spacing of 170 mm in vacuum under nanosecond quasi-square pulses is studied by the imaging system, and the change of luminosity is analyzed during the surface flashover process.

Keywords: A-K gap; High speed framing camera; Imaging system; Intense electron-beam accelerator; Plasma

1. INTRODUCTION

High speed framing camera (HSFC) is widely used in the areas of hypervelocity impact studies, ultrasonic flame propagation, laser ablation, sparks in electrical switches, and short time physics (Koing *et al.*, 2005; Mark *et al.*, 2010; Sun *et al.*, 2013; Yang *et al.*, 2013). So in the field of intense electron beam accelerator (IEBA), HSFC could be assembled to visualize the evolution of discharging and plasma generation phenomenon in nanosecond regime. IEBA based on Blumlein pulse forming line (BPFL) and high voltage pulse transformer (HVPT) is usually used to generate high voltage pulse with duration of hundreds of nanosecond (Friedman *et al.*, 1988; Katsuki *et al.*, 2001; Kumar *et al.*, 2008; Liu *et al.*, 2009), and which is widely used is in a great variety of applications such as in high power pulsed lasers (Apruzese *et al.*, 2006; Sethian *et al.*, 2000), X-ray generation (Tarasenko *et al.*, 2005; Kuai *et al.*, 2009), and high power microwave generators (HPMG) (Steven & Gregory, 1997; Zhang *et al.*, 2004) and so on. In these applications of IEBA, the output pulse of IEBA is used to drive cold cathode and generate electron beams (Miller *et al.*, 1998). For example, electron-beam (e-beam)-pumped high-power KrF laser that is performed by Naval Research Laboratory of USA requires 500 kV, 110 kA, 100 ns flat-top electron beams (Frank *et al.*, 2008; Sethian *et al.*, 2000). Now, velvet, graphite, and carbon fiber are the common cathode material of vacuum diode to generate intense electron beams. Meanwhile, to generate the high-current electron beams and satisfy the need of application, the cathode material should have the characteristics of low electric-field threshold for plasma initiation, highly uniform emission, low plasma expansion velocities and a long life-time (Li *et al.*, 2008). So, it is very important to investigate the emission characteristics of cathode material. Luckily, the HSFC could be used to visualize the evolution of discharging (Laity *et al.*, 2011; Neuber *et al.*, 1999) and plasma generation phenomenon (Tiwari *et al.*, 2012; Walter *et al.*, 2008), so it could be assembled to capture the image of the

Address correspondence and reprint requests to: Jin-Liang Liu, College of Optoelectronic Science and Engineering, National University of Defense Technology, Changsha, Hunan, Peoples Republic of China 410073. E-mail: ljle333@yahoo.com

electron beams and to investigate the emission characteristics of vacuum diode.

However, to use the HSFC in the field of the IEBA successfully, the synchronism problem of HSFC should be taken into account carefully for that the inherent delay time (IDT) of HSFC, which is defined as the time between the start of trigger signal and the shutter open of the HSFC is unavoidable, and the choice of the trigger signal source of the HSFC is decided the diagnosis results of the electron beams directly on the IEBA. Now, if the load voltage of IEBA that is used to generate electron beam is used as trigger signal source, and to compensate the time (called compensated time), which is defined the sum of the trigger signal processing time and the IDT of the HSFC, there are two basic methods to realize the synchronization between HSFC and IEBA. One is the optical delay method, and the other is the electrical delay method. For the optical delay method, the light radiated from the electron beam is delayed. However, if the compensated time to synchronize the HSFC is long, bigger the diverging angle of light beams and lowers the quality of the imagery for the longer light path. For example, if the compensated time is 30 ns, the light path should be up to 9 m, which lead to a poor imaging quality. For the electrical delay method, a transmission line (TL) is usually used to delay the time of the electron emission, and the transmission time of TL should be larger than the compensated time (Yang *et al.*, 2013). Obviously, for different accelerator, the TL should be redesigned to match the accelerator. So, to synchronize HSFC and IEBA easily, the trigger signal source must be re-chosen, and the electrical delay method is usually adopted.

So in this paper, we mainly discuss the method of HSFC's application on the IEBA, and give some results of the HSFC's application. Section 2 introduces the HSFC, structure, and operation process of IEBA. To use the HSFC, synchronization between HSFC and IEBA is very important, so a synchronization trigger method is introduced in Section 3. Subsequently, the application of HSFC is presented in Section 4, which is used to obtain the images of the emission images of a stainless steel cathode and the vacuum surface flashover. Finally, Section 5 summarizes the conclusions of this paper.

2. OVERVIEW OF HSFC AND IEBA

2.1. HSFC System

The HSFC (PCO Computer Optics GmbH) system used in this paper has been shown in Figure 1, which comprises an input lens (Nikon F-Mount lens), optical beam splitter, four intensified charge-coupled-device (CCD) camera modules with fast switchable micro channel plate(MCP) image intensifiers and high resolution CCD image sensors, and personal computer (PC). Each module with its 12 bit dynamic range and a high resolution CCD image sensor features an excellent signal-to-noise-ratio and the ability of single photon detection. Four high speed serial fiber optic data links connect the HSFC to the PCI-Interface-Boards which are placed in the PC. The HSFC can obtain four frames imaging for every operation, and it can be triggered externally by light or electrical input. For electrical trigger, a TTL signal (5 V) with rising edge is required and the rise time should be less than 20 ns. For light trigger, the trigger signal has to last for a minimum of 10 ns with light power of 1 mW. In the paper, the electrical trigger is adopted, so an electrical trigger module should be designed to trigger the HSFC.

The operation progress of the HSFC system is as follow. First, putting the electrical trigger signal into the HSFC, then, after the IDT of HSFC the shutter is open. Subsequently, the light is coupled into the HSFC by the input lens, and divided into four light beams by optical beam splitter. Next, the four light beams are transmitted into the MCP image intensifiers and high resolution CCD image sensors which are used to imaging the light. At last, the images are display on the PC by the data format conversion of PCI-Interface-Boards.

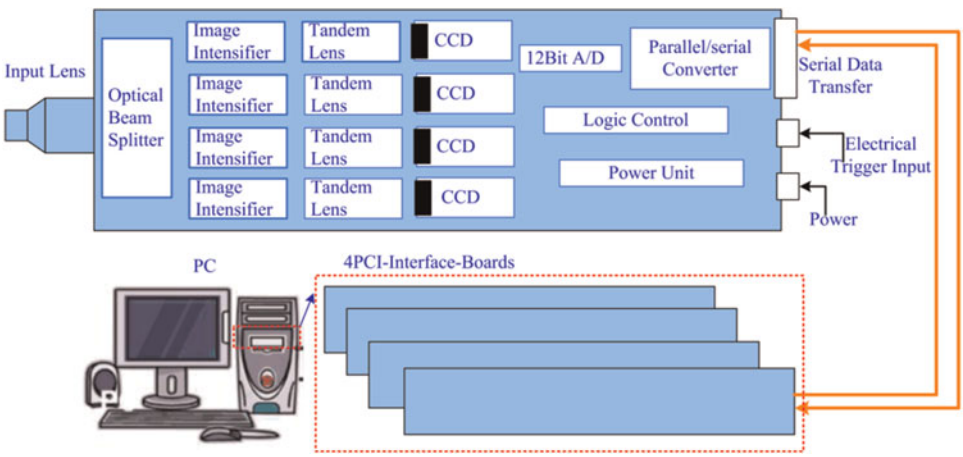

Fig. 1. (Color online) Schematic diagram of the HSFC system.

https://doi.org/10.1017/S0263034613000633 Published online by Cambridge University Press

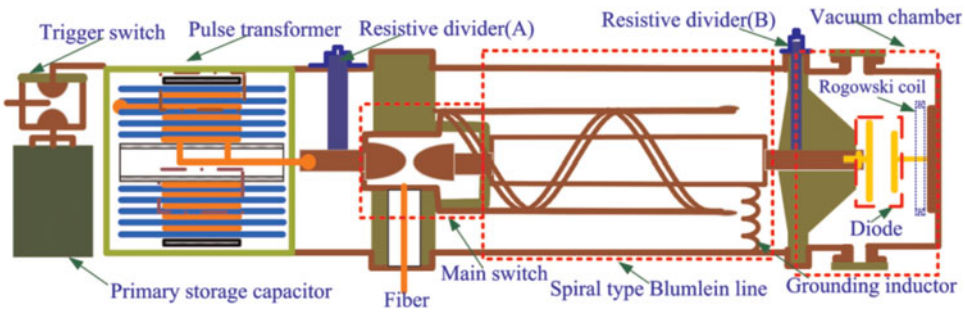

Fig. 2. (Color online) Structure of the IEBA.

Meanwhile, the IDT is about 48 ns when the HSFC operates at single exposure mode. So to diagnostic the discharging process, the electrical trigger module should have the function to realize the synchronization of the HSFC and IEBA. In other words, the time between the electrical trigger signal of HSFC and the electron beam should be larger than 48 ns.

2.2. IEBA Configuration

Figure 2 shows the typical structure of IEBA based on pulse transformer and BPFL, which mainly consisted of a 50 kV, 12 μF primary storage capacitor, a 50 kV field distortion trigger switch (Cheng *et al.*, 2010), a spiral strip type pulsed transformer with output voltage up to 600 kV (Liu *et al.*, 2007), main switch with sulfur-hexafluoride (SF_6) used as insulating medium, strip spiral type BPFL with impedance of about 10 Ω, vacuum chamber which was pumped by the combination of mechanical and molecular pumps to keep the vacuum degree up to 10^{-3} Pa, voltage and current diagnostic system. To generate the electron beam, a field-emission diode is usually placed in the vacuum chamber.

The operating process of the IEBA is as follow. First, a constant-current charging system (not shown in Fig. 2) is used to charge the primary storage capacitor. When the charging voltage of the primary storage capacitor reaches to a certain value, the field distortion trigger switch is triggered and closed, and then the primary storage capacitor discharges to the primary winding of the pulse transformer consequently, the transformer starts to charge the Blumlein PFL. Once the charging voltage of the Blumlein PFL reaches the breakdown value of the main switch, the BPFL discharges to the load, and a quasi-square wave with a rise time approximately 30 ns and full width at half maximum of 180 ns is formed on the load. The amplitude of the quasi-square wave could be adjusted from 100 kV to 500 kV by changing the gas pressure ($Pm = 0$–0.50 MPa) of the main switch, so the output peak power could be up to 30 giga-watt.

3. SYNCHRONIZATION OF HSFC AND IEBA

To actualize the synchronization trigger between the HSFC and IEBA, the choice of the trigger signal source is very important. Figure 3 shows the time series of the operation progress of the electrical trigger module

Once the trigger signal source is decided, the delay time between the trigger signal source and the discharging progress (T_T) must be bigger than the sum of the cable delay (T_C), signal processing delay (T_S) and IDT of HSFC (T_{IDT}), and the delay time between the electrical trigger signal and the discharging progress should be bigger than 48 ns ($T_T > T_C + T_S + T_{IDT}$, and $T_T - T_C - T_S > 48\,ns$). So in Figure 2, if the load voltage which is measured by the Resistive divider (B) is used as the trigger signal source, a TL must be added between the diode and the BPFL, and the transmission time of TL is larger than 48 ns at least. According to characteristic of TL[28], $t = l\sqrt{\varepsilon_r}/c$ (t is the transmission time, l is the length of the TL, ε_r is the relative permittivity of the dielectric medium in the TL, and c is the light velocity), if the water used as the dielectric medium (ε_r =81), the length of the TL must be longer than 1.6 m. Meanwhile, the impedance of TL is difficult matched with that of the BPFL. So, the load voltage is an inappropriate trigger signal source.

Meanwhile, in Figure 2, the voltage measured by resistive divider (B) is the breakdown voltage of the main switch. According to the theory of BPFL, the main pulse is formed after the main switch closing with a delay time of single pulse forming line (Pai & Zhang, 1995). In other words, for an IEBA with duration of 180 ns, the delay time is about 90 ns, which is larger than the IDT of HSFC. So the breakdown voltage of the main switch is an ideal trigger signal source to trigger the HSFC. However, the jitter of the breakdown voltage is usually very large, especially self-breakdown main switch, which make the synchronization

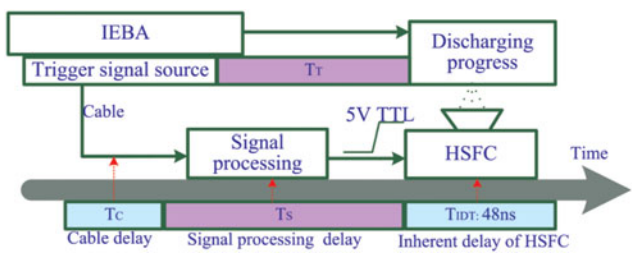

Fig. 3. (Color online) Time series of the operation progress of the electrical trigger module.

https://doi.org/10.1017/S0263034613000633 Published online by Cambridge University Press

unstable. Further, the breakdown voltage is usually about hundreds of kilovolts, to satisfy the need of the HSFC, it need to be converted to a TTL signal (5 V), the processing circuit is complex. However, according to the test of the light signal in this paper, during the switch closing, the light radiated from the main switch of IEBA is very stable, and the amplitude of the voltage outputted from the optical-electrical converter is about 0.8 V, which is easily converted to a 5V TTL signal. So a novel method based on the light signal is proposed to realize the synchronization trigger between HSFC and IEBA (Cheng *et al.*, 2012*a*).

The novel electrical trigger module of HSFC includes optical fiber, avalanche photodiode (APD) module and a signal processing module, which is shown in Figure 4. When the main switch of the IEBA is closed, the optical fiber in Figure 2 is used to collect the light signal which radiated from the main switch. Subsequently, the light signal is coupled into the APD module from the optical fiber, and then the output voltage of APD is input a signal processing module, an electrical trigger signal could be outputted from the signal processing module and be used to trigger the HSFC. In Figure 4, the delay time between the electrical trigger signal outputted from the signal processing module and the discharging progress must be bigger than the IDT of HSFC of about 48 ns.

To test the electrical trigger module of HSFC, a high power water load is used instead of the field-emission diode in Figure 2, and the "water" is a solution of CuSO4 of a concentration that is adjusted to match the impedance of the Blumlein PFL. Figure 5 shows the typical waveform of the load voltage and electrical trigger signal of HSFC outputted from the electrical trigger module. It is shown that

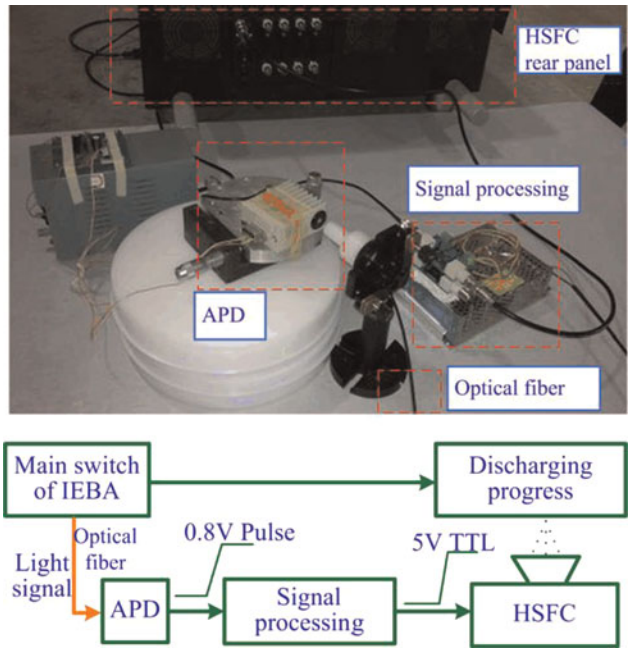

Fig. 4. (Color online) The operation principle of electrical trigger module of HSFC.

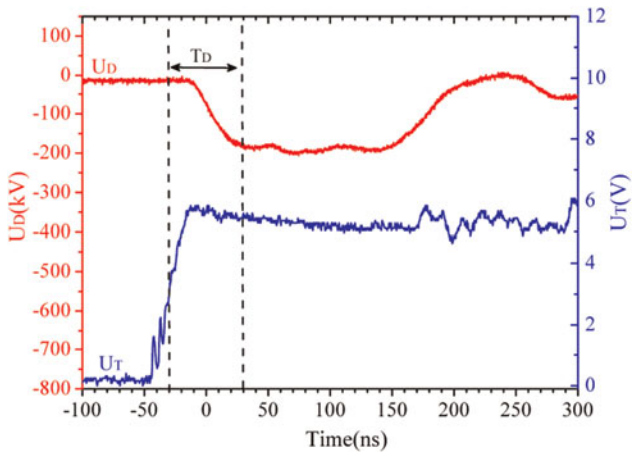

Fig. 5. (Color online) Typical waveform of load voltage and electrical trigger signal of HSFC.

the electrical trigger module could provide a trigger signal with rise time of 17 ns and amplitude of about 5 V, the delay time between the high level voltage (3 V) of electrical trigger signal and the start of the flat-top of load voltage is about 60 ns, which is bigger than the IDT of HSFC of about 48 ns. So the electrical trigger module could realize the synchronization trigger between HSFC and IEBA.

4. APPLICATION OF HSFC ON IEBA

4.1. Optical Characteristics of Gap Closure of Short Gap Vacuum Diode

In the field of IEBA, the vacuum diode is used to generate electron beams, and the phenomenon of gap closure of the vacuum diode should be avoided, which adversely affects the diode performance, limits the duration of the electron beam pulse, and results in poor efficiency of coupling between the electron beam diode and the IEBA (Roy *et al.*, 2009). So the gap closure of diode is widely researched (Li *et al.*, 2008; Robert *et al.*, 2001; Sampayan *et al.*, 1990). In this part, the optical characteristics of a short gap diode with the condition of gap closure are investigated by HSFC.

The schematic diagram of the experimental system is shown in Figure 6. The experimental configuration consisted of an IEBA, an electrical trigger modular, HSFC, vacuum chamber and oscilloscope (LeCroy, 44MXs-B, 400MHz, and 5GS/s). If a matched load is used, the output pulse of IEBA is a quasi-square pulse with duration of 180 ns. A turbo-molecular pump (not shown in Fig. 6) mounted directly on the vacuum chamber used to evacuate the diode region, and the vacuum chamber is pumped to a vacuum pressure of 10^{-5} Torr. Before the experiments, a 5 mm anode-cathode (A-K) gap is placed in the vacuum chamber of the IEBA, one of the pair of stainless steel electrodes with a diameter of 60 mm is grounded and a pulse with duration of 180 ns outputted from the IEBA is applied to the

https://doi.org/10.1017/S0263034613000633 Published online by Cambridge University Press

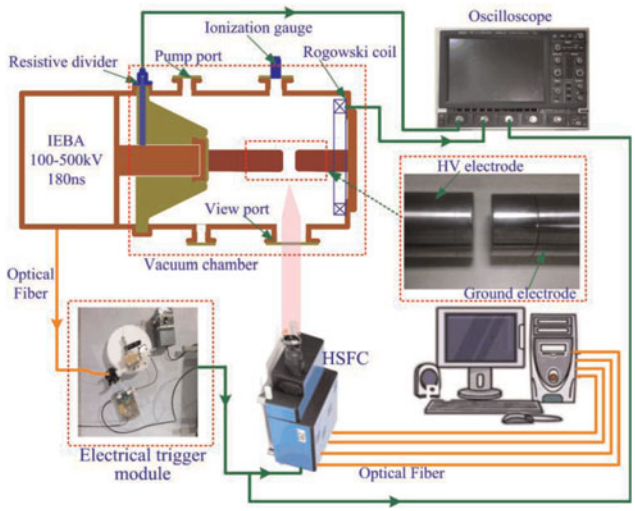

Fig. 6. (Color online) Schematic diagram of the experiment setup.

other stainless steel electrodes. The diode voltage was monitored by a resistive divider and the electron beam current was measured with a Rogowski coil. Plasma images of the short A-K gap region were observed by the HSFC, and the electrical trigger modular is used to realize the synchronization of HSFC and IEBA. Meanwhile, the load voltage, electron beam current and the electrical trigger signal of HSFC are all monitored by the oscilloscope.

Figure 7 shows the typical waveforms of trigger signal of HSFC, diode voltage, and diode current. First, if a high power water load with impedance of 10 Ω is used instead of the vacuum diode, the measured voltage by the resistive divider is a quasi-square pulses with voltage amplitude of about 210 kV, duration of 180 ns and flat-top time of 110 ns. Then, the 5 mm A-K gap is placed in the vacuum chamber and used as the load of IEBA. The waveform of the measured voltage is changed obviously, and the plat-top time is decreased to about 50 ns. At the time of 70 ns, the voltage starts to decrease. Here the current density is determined by the well-known Child–Langmuir law $J_e(t) = (4e_0/9)\sqrt{2e/m}(U_D(t)^{3/2}/d^2)$, where $U_D(t)$ is the diode voltage and d is the A–K gap, e and m are the electron charge and mass, e_0 is the free space permittivity. Thus, at the same A-K gap, the diode voltage is an important factor affecting the current density. In Figure 7, at time of 20 ns, the diode current starts to increase.

After the A-K gap is placed in the vacuum chamber, the flat-top time of the diode voltage is reduced to only about 50 ns. The main reason is the gap closure of the diode. During the operation of IEBA, the diode voltage begins to increase and electrons are emitted from the stainless steel cathode by field emission. Then, the electrons expand along the axial direction within the diode region. For the gap spacing of the A-K gap is only 5 mm, so the time of the gap closure is very short, and the impedance of the diode is reduced quickly. Meanwhile, the flat-top time of the diode voltage is also reduced, which is caused by the gap closure. After the gap closure, the impedance of the diode is inductive and waveform of the diode voltage is mainly decided by the inductance of the diode region (L_D). So $U_D(t) = R_D I_D(t) + L_D \dfrac{dI_D(t)}{dt}$, where R_D is the resistance of the diode after the gap closure.

Sweeping the inductance of the diode region and comparing with the waveform of the experimental measured voltage, the inductance of the flashover channel could be obtained after the gap closure. Figure 8 shows the waveforms of experimental measured voltage, diode current, and theoretical calculated voltage waveforms when the gap closure occurs with inductance of the diode region of 250 nH. In Figure 8, it is shown that after the formation of the flashover channel, the waveform of theoretical calculated voltage is almost the same as that of the experimental measured voltage. So the inductance of the diode region is about 250 nH after the gap closure.

To further show the gap closure, the purveyance for the electron flow in the A-K gap region of the diode can be defined by $P_P(t) = I_D(t)/V_D(t)^{3/2}$. Then the experimental purveyance can be obtained in Figure 9. It was shown that the

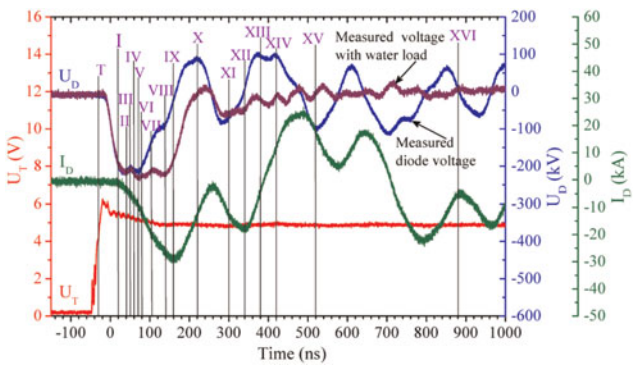

Fig. 7. (Color online) Typical waveforms of trigger signal of HSFC (U_T), experimental measured voltage waveform (U_D), diode current (ID), and the time series of HSFC to image the optical emission from the vacuum diode.

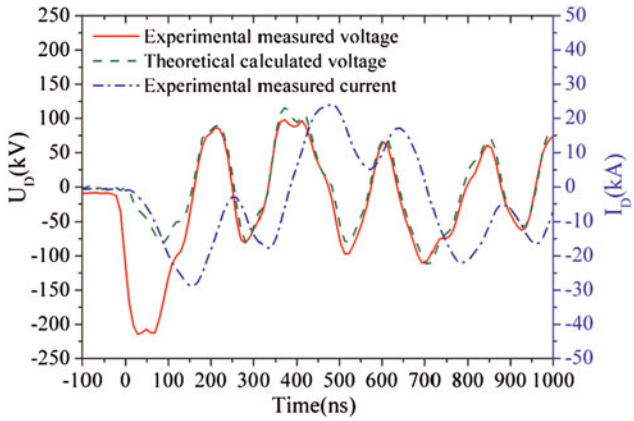

Fig. 8. (Color online) Waveforms of experimental measured voltage and theoretical calculated voltage when the gap closure occurs.

https://doi.org/10.1017/S0263034613000633 Published online by Cambridge University Press

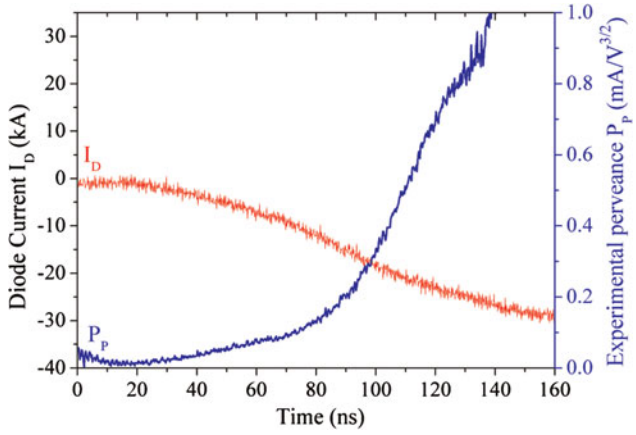

Fig. 9. (Color online) Experimental perveance for the electron flow in the 5 mm A-K gap region of the diode

diode purveyance increases rapidly after 100 ns showing gap closure.

To obtain the developmental process of the plasma in the vacuum diode region, HSFC is used to capture the plasma images. Note that the HSFC can only obtain four frames imaging for every discharge, so to image the whole process of optical emission from the vacuum diode, a train of images should be constructed from multiple discharges in a series of trials. Since the diode exhibit steady repeatability under a high enough applied voltage, the growing process of the diode plasma can be constructed from multiple discharges in a series of trials.

In this study, the HSFC was gated for a 3 ns exposure, and according to the time series in Figure 7, images of growing process of the diode plasma were shown in Figure 10 and the luminosity of all images was normalized. First, at time of −31 ns, HSFC was triggered, and after a delay time of about 48 ns, the shutter of HSFC was opened, the first image was recorded (inset I in Fig. 10). Now, the time is 20 ns, and the diode current is about zero, so, there is no obviously luminous spot. Subsequently, at 40 ns (inset II in Fig. 10), electrons is emitted from the cathode surface, and the light emission is not uniform, there is only a bright spot. As the diode voltage proceeded, brighter and larger emission center along the periphery of the cathode appeared, and weak emission at the cathode center was also observed (insets III and IV in Fig. 10), it is caused by the electrical field enhancement at the cathode periphery. Also, the diode current was increased. Next, at 105 ns (inset VII in Fig. 10), the light had been filled the A-K gap region, it means that the A-K gap had been closed. Meanwhile, the diode voltage in Figure 7 starts to decrease. As the gap closure of the diode, the impedance of the diode is reduced, so the diode current keeps on increasing and the luminosity in the A-K gap region becomes stronger.

However, at 160 ns, the diode voltage reduced to zero and the diode current reached to the maximum of −28 kA. Also, the light in the A-K gap region was much brighter (inset IX in Fig. 10). Then, the diode voltage was changed from a negative voltage to a positive voltage (peak value is 90 kV), the electrons that moved to the anode were decelerated, and some electrons emitted from the anode and moved to the cathode. So the anode plasma and cathode plasma would have an effect on the diode current and light luminosity, resulting in the diode current decreased and the light in the A-K gap region turn weaker (insets X and XI in Fig. 10). At 250 ns, the diode voltage was changed to zero again, the diode current changed to the minimum value of −2 kA. At the same time, the diode voltage is changed from positive voltage to negative voltage, the electrons that moved to the anode were accelerated and more electrons

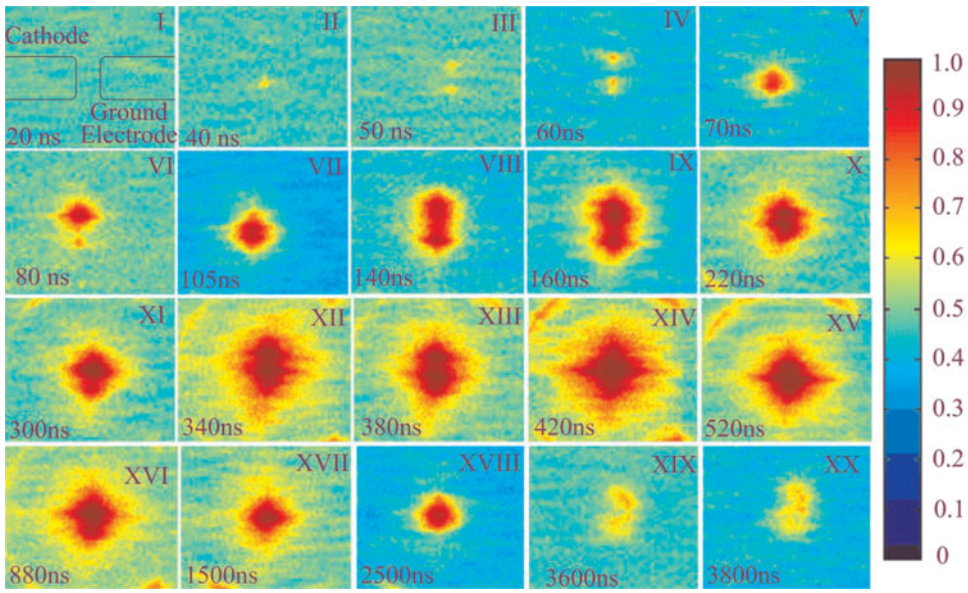

Fig. 10. (Color online) HSFC images of light emission from the 5 mm A-K gap region.

https://doi.org/10.1017/S0263034613000633 Published online by Cambridge University Press

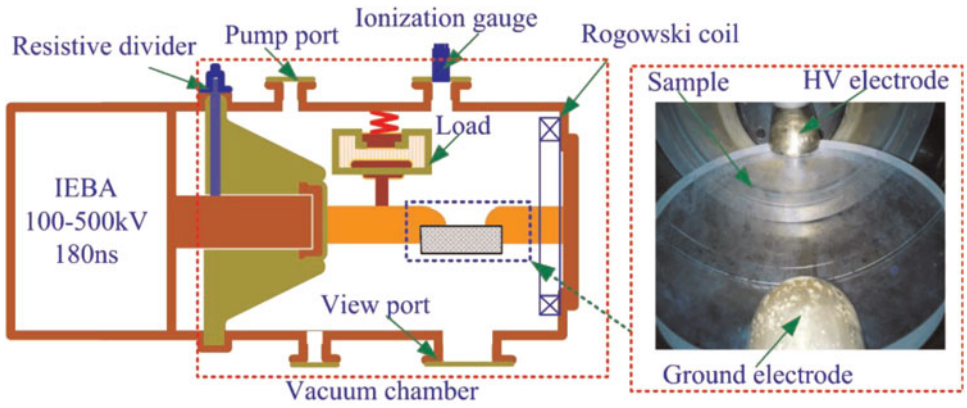

Fig. 11. (Color online) Schematic diagram of the vacuum chamber during the investigation of the surface flashover.

emitted from the cathode again, so the diode current started to increase to the maximum of −17.5 kA, and the luminosity in the A-K gap region turn stronger (inset XII in Fig. 8). According to the results in Figures 7 and 10, after 300 ns, as the change of the load voltage, the luminosity in the A-K gap region was changed. At 420 ns, the luminosity was the strongest (inset XIV in Fig. 10), and then, the light emission turn weaker. After about 3800 ns, the light emission was disappeared. In a word, the light emission in the A-K gap region may be decided by the competition between the cathode plasma and anode plasma, which was caused by the change of the load voltage. Meanwhile, according to Figures 7 and 10, the gap is closed at 100 ns, and the current starts to increase at about 20 ns, so the plasma expansion velocity could be about 6.25 cm/μs.

So, under long pulse operation, the short A-K gap is closed prematurely. The light emission in the A-K gap region has the characteristics of "re-ignition" caused by the competition between the cathode plasma and anode plasma. The light emission begins with a weaker luminosity, and then luminosity becomes strongest. Next, the luminosity will reduce, and then the luminosity increase again. After the repeated progress, the light emission is disappeared, and the light duration time is very long (about 3800 ns in the experimental results).

4.2. Optical Characteristics of Vacuum Surface Flashover Channel

As the development of the IEBA, surface flashover (i.e., voltage breakdown along the surface of insulator) phenomenon of insulator is the one of the main factors that restricts the improvement of the operating voltage and decrease of the size of IEBA. Especially in vacuum, the insulator surface strength is only one-tenth of the breakdown strength of the vacuum gap or bulk breakdown strength of the insulator itself in the same dimension (Miller, 1989). Meanwhile, in the IEBA, vacuum diodes are among the most important parts of IEBA. It converts several converts several hundred kilovolt and nanosecond voltage pulse into relativistic electron beams (Xun *et al.*, 2008). Insulators in diodes make a function of supporting significant voltage while exposed to vacuum, and surface flashover of the insulator must be avoided. So the surface flashover characteristics of insulator in vacuum under hundreds of nanosecond pulse should be investigated. In this part, the optical characteristic of surface flashover channel of poly-methyl methacrylate (PMMA) is introduced with the help of HSFC (Cheng *et al.*, 2012*b*).

To investigate the vacuum surface flashover under hundreds of quasi-square pulse by using the HSFC, the experiment setup is almost the same as that in Figure 6, and the only difference is the vacuum chamber. Figure 11 shows the structure of the vacuum chamber during the investigation of the surface flashover. One of the pair of finger-shaped brass electrodes is grounded and a quasi-square pulse with duration of 180 ns outputted from the IEBA is applied to the other figure-shaped electrodes. Meanwhile, a discoid PMMA insulator is placed between the two electrodes and the gap length between the two electrodes is 170 mm. During the experiments, the vacuum chamber is pumped to a vacuum pressure of 10^{-4} Torr and the discharge propagation is observed by the HSFC. Meanwhile, the surface

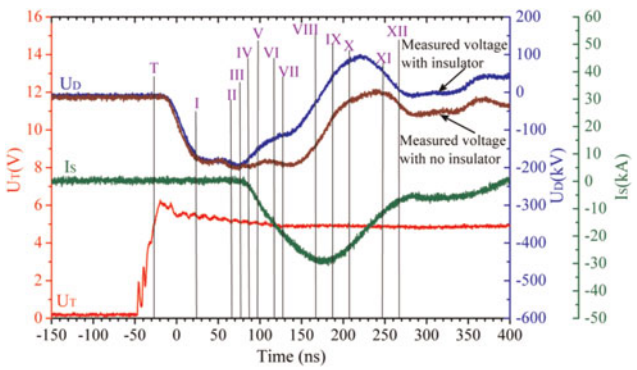

Fig. 12. (Color online) Typical waveforms of trigger signal of HSFC (U_T), experimental voltage (U_D) measured by resistive divider, surface flashover current (I_S) measured by Rogowski coil, and the time series of HSFC to image the optical emission from the surface flashover event.

https://doi.org/10.1017/S0263034613000633 Published online by Cambridge University Press

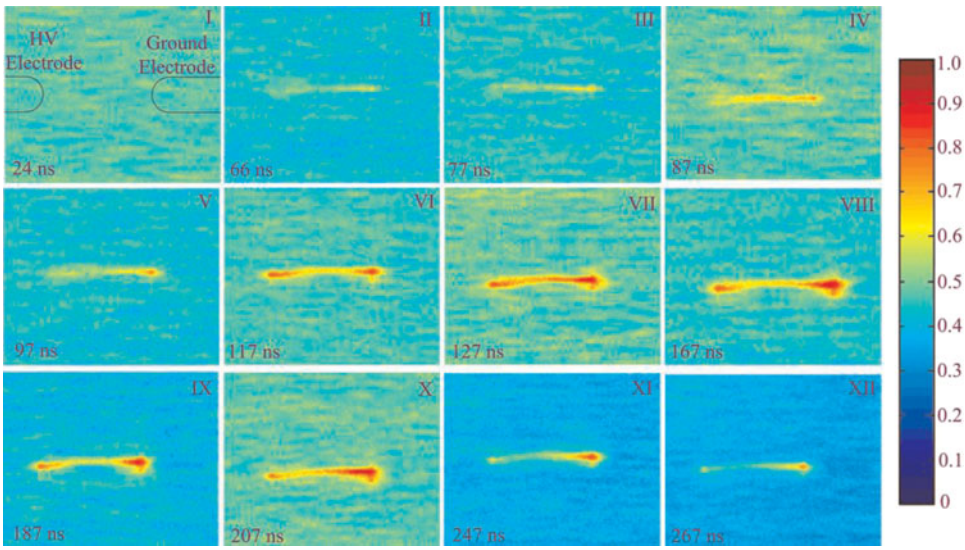

Fig. 13. (Color online) HSFC images of growing process of surface flashover of PMMA insulator.

flashover current and the voltage are also measured by the Rogowski coil and resistive divider, respectively.

Figure 12 shows the typical waveforms of trigger signal of HSFC, experimental measured voltage, and surface flashover current. It is clearly shown that before adding the PMMA insulator the experimental measured voltage is a quasi-square pulses with voltage amplitude of about 190 kV and duration of 180 ns. However, after adding the insulator, the waveform of the measured voltage is changed, obviously, at the time of 80 ns, the voltage starts to decrease, meanwhile, the flashover current starts to increase.

In this study, the HSFC was gated for a 3 ns exposure, and according to the time series in Figure 12, images of growing process of the surface flashover channel were shown in Figure 13 and the luminosity of all images was normalized.

First, at time of −27 ns, HSFC was triggered, and after a delay time of about 48 ns, the shutter of HSFC was opened, the first image was recorded (inset I in Fig. 13). Now, the time is 24 ns, and the flashover current is zero, so, there is no obviously luminous spot. Subsequently, at time of 66 ns (inset II in Fig. 13), the current measured by the Rogowski coil is still about zero, but filament current channel appears. It is because the Rogowski coil could only test the current that pass through it. Next, the flashover current starts to increase, and the luminosity of the flashover channel becomes stronger. Obviously, the closer the ground electrode, the stronger the luminosity, it is because that some of the electrons field-emitted from the triple junction (electrode-insulator-vacuum) impact upon the surface of the insulator producing additional electrons by secondary emission. Some of these secondary electrons will again strike the insulator surface, producing tertiary electrons. So, the electrons are accumulated at the top of the flashover channel (near the ground electrode). Next, the voltage was decreased, but the field emission from the high voltage (HV) electrode near the triple junction still replenished the electrons in the flashover channel. So the luminosity near the HV electrode became stronger. Of course, the flashover current was increased. At time of 127 ns (inset VII in Fig. 13), the luminosity of entire channel was homogeneous. Subsequently, at time of 167 ns, the luminosity is the most strongest, so the flashover channel was totally formed. Then, the luminosity of flashover channel turns weaker. However, the luminosity near the HV electrode turns weaker quickly. At time of 247 ns (inset XI in Fig. 13), the flashover channel becomes very thin, and the luminosity near the HV electrode is very weak.

In a word, surface flashover begins with a luminous front traveling from the HV electrode to the ground electrode. When this luminosity reaches the ground electrode, then a much brighter luminosity starts from the ground electrode and proceeds to the HV electrode. Meanwhile, the flashover channel is changed from a thin line to a thick line. Subsequently, when the flashover current starts to decrease, the luminosity of the flashover channel starts to decrease and the luminosity near the HV electrode decreases quickly.

5. CONCLUSIONS

In conclusion, we have presented an overview of the application of HSFC on the IEBA. HSFC is a useful tool to visualize the evolution of discharging and plasma generation phenomenon, and IEBA is usually to generate electron beams, so the HSFC could be used to visualize the evolution of the electron beams on IEBA. However, to use the HSFC successful, the synchronization trigger between the HSFC and IEBA is a primary problem, so we introduce several kinds of synchronization trigger method in this paper firstly. In particular, based on the characteristics of the BPFL and IEBA, a simple and novel synchronization trigger system is presented and experimentally demonstrated. The synchronization trigger system which include light signal acquisition radiated from main switch of IEBA and signal processing

https://doi.org/10.1017/S0263034613000633 Published online by Cambridge University Press

circuit could provide a trigger signal with rise time of 17 ns and amplitude of about 5 V, and the delay time between the high level voltage (3 V) of electrical trigger signal and the start of the flat top of load voltage is about 60 ns, which is bigger than the IDT of HSFC of about 48 ns.

Furthermore, an imaging system based on IEBA, HSFC and the synchronization trigger system is developed, and it can be used to image the developmental process of plasma in the output vacuum chamber of IEBA and to measure the electrical parameter of IEBA and electrical trigger signal in real time. Firstly, the imaging system is used to investigate the gap closure of a 5 mm A-K gap. The developmental process of electron beam of the A-K gap in vacuum under 180 nanosecond quasi-square pulses is investigated in detail, and the change of luminosity is analyzed during the operation of the A-K gap. According to the results, it is obtained that the short A-K gap is closed prematurely under long pulse operation with plasma expansion velocity of about 6.25 cm/μs and the light emission in the A-K gap region has the characteristics of "re-ignition" with light duration time about 3800 ns. Secondly, the developmental process of surface flashover channel of PMMA insulator with gap spacing of 170 mm in vacuum under nanosecond quasi-square pulses is studied by the imaging system, and the change of luminosity is analyzed during the surface flashover process.

ACKNOWLEDGMENTS

This work is in part supported by the fund of innovation, Graduate School of National University of Defense Technology (B090701), and National Natural Science Foundation of China (51177167). The authors also wish to thank Dr. Jie Yang for his assistance in the experiment of HSFC application.

REFERENCES

Apruzese, J.P., Giuliani, J.L.,Wolford, M.F., Sethian, J.D., Petrov, G.M., Hinshelwood, J.D., Myers, M.C. & Ponce, D.M. (2006). Experimental evidence for the role of Xe^{2+} pumping the Ar-Xe infrared laser. *Appl. Phys. Lett.* **88**, 121120.

Cheng, X.B., Liu, J.L., Qian, B.L., Chen, Z. & Feng, J.H. (2010). Research of a high current repetitive triggered spark gap switch and its application. *IEEE Trans. Plasma Sci.* **38**, 16–22.

Cheng, X.B., Liu, J.L., Hong, Z.Q. & Qian, B.L. (2012*a*). Synchronization of high speed framing camera and intense electron-beam accelerator. *Rev. Sci. Instrum.* **83**, 065104.

Cheng, X.B., Liu, J.L. & Qian, B.L. (2012*b*). Characteristics of long gap surface flashover channel in vacuum under nanosecond quasi-square pulses. *Appl. Phys. Lett.* **101**, 08290.

Frank, H., John, L.G., John, D.S., Matthew, C.M., Patrick, M.B. & Moshe, F. (2008). Forced convective cooling of foils in a repetitively pulsed electron-beam diode. *IEEE Trans. Plasma Sci.* **36**, 778–793.

Friedman, S., Limpaecher, R. & Sirchis, M. (1988). Compact energy storage using a modified-spiral PFL. In *Power Modulator Symposium*. New York: IEEE.

Katsuki, S., Takano, D., Namihira, T. & Akiyama, H. (2001). Repetitive operation of water-filled Blumlein generator. *Rev. Sci. Intrum.* **72**, 2759–2763.

Koing, J., Nolte, S. & Tunnermann. (2005). Plasma evolution during metal ablation with ultrashort laser pulses. *Opt. Express* **13**, 10597–10607.

Kuai, B., Wu, G., Qiu, A., Wang, L., Cong, P. & Wang, X. (2009). Soft X-ray emissions from neon gas-puff Z-pinch powered by Qiang Guang-I accelerator. *Laser Part. Beams* **27**, 569–577.

Kumar, R., Novac, B.M., Sarkar, P., Simith, I.R. & Greenwood, C. (2008). 300 kV Tesla transformer based pulse forming line generator. Proceedings of the 2008 IEEE International Power Modulators and High Voltage Conference. Las Vegas, NE, 246–249.

Laity, G.R., Fierro, A.S., Hatfield, L.L., Dickens, J.C. & Neuber, A. (2011). Spatially resolved VUV spectral imaging of pulsed atmospheric flashover. *IEEE Trans. Plasma Sci.* **39**, 2122–2123.

Li, L.M., Wen, J.C., Men, T. & Liu, Y.G. (2008). An intense-current electron beam source with low-level plasma formation. *J. Phys. D: Appl. Phys.* **41**, 125201.

Liu, J.L., Zhan, T.W., Zhang, J., Liu, Z.X., Feng, J.H., Shu, T., Zhang, J.D. & Wang, X.X. (2007). A Tesla pulse transformer for spiral water pulse forming line charging. *Laser Part. Beams* **25**, 305–312.

Liu, J.L., Cheng, X.B., Qian, B.L., Ge, B., Zhang, J.D. & Wang, X.X. (2009). Study on strip spiral Blumlein line for the pulsed forming line of intense electron-beam accelerators. *Laser Part. Beams* **27**, 95–102.

Mark, P., Brian, J. & Anthony, W. (2010). Three-dimensional digital image correlation technique using single high-speed camera for measuring large out-of-plane displacements at high framing rates. *Appl. Opt.* **49**, 3418–3427.

Miller, H.C. (1989). Surface flashover of insulators. *IEEE Trans. Elect. Insul.* **24**, 765.

Miller, R.B. (1998). Mechanism of explosive electron emission for dielectric fiber (velvet) cathodes. *J. Appl. Phys.* **84**, 3880–3889.

Neuber, A., Hemmert, D., Dickens, J., Krompholz, H., Hatfield, L. L. & Kristiansen, M. (1999). Imaging of high-power microwave-induced surface flashover. *IEEE Trans. Plasma Sci.* **27**, 138–139.

Pai, S.T. & Zhang, Q. (1995). *Introduction to High Power Pulse Technology*. Singapore: World Scientific.

Robert, J.B. & Edl, S. (2001). *High Power Microwave Sources and Technologies* Beijing: Tsinghua University Press.

Roy, A., Menon, R., Mitra, S., Kumar, S., Sharma, V., Nagesh, K.V., Mittal, K.C. & Chakravarthy, D.P. (2009), Plasma expansion and fast gap closure in a high power electron beam diode. *Phys. Plasmas* **16**, 053103.

Sampayan, S.E., Gurbaxani, S.H. & Buttram, M.T. (1990). Plasma-cathode-initiated vacuum gap closure. *J. Appl. Phys.* **68**, 2058.

Sethian, J.D., Myers, M., Smith, I.D., Carboni, V., Kishi, J., Morton, D., Pearce, J., Bowen, B., Schllitt, L., Barr, O. & Webster, W. (2000). Pulsed power for a rep-rate, electron beam pumped KrF laser. *IEEE Trans. Plasma Sci.* **28** 1333–1337.

Steven, H.G. & Gregory, S.N. (1997). Review of high-power microwave source research. *Rev. Sci. Instrum.* **68**, 3945–3974.

Sun, Z.W., Zhu, J.J., Li, Z.S., Alden, M., Feipold, F., Salewski, M. & Kusano, Y. (2013). Optical diagnostics of a gliding arc. *Opt. Express* **21**, 6028–6044.

Tarasenko, V.F., Shunailov, S.A., Shpak, V.G. & Kostyrya, I.D. (2005). Super short electron beam from air filled diode at atmospheric pressure. *Laser Part. Beams* **23**, 545–551.

Tiwari, N., Sahasrabudhe, S.N., Tak, A.K., Barve, D.N. & Das, A.K. (2012). Investigations of some aspects of the spray process in a single wire arc plasma spray system using high speed camera. *Rev. Sci. Instrum.* **83**, 025110.

Walter, J., Mankowski, J. & Dickens, J. (2008). Imaging of the explosive emission cathode plasma in a vircator high-power microwave source. *IEEE Trans. Plasma Sci.* **36**, 1388–1389.

Xun, T., Yang, H.W., Zhang, J.D., Liu, Z.X., Wang, Y. & Zhao, Y.S. (2008). A ceramic radial insulation structure for a relativistic electron beam vacuum diode. *Revs. Sci. Instrum.* **79**, 063303.

Yang, J., Shu, T. & Fan, Y.W. (2013). Time evolution of the two-dimensional expansion velocity distributions of the cathode plasma in pulsed high-power diodes. *Laser Part. Beams* **31**, 129–134.

Zhang, J., Zhong, H.H. & Luo, L. (2004). A novel overmoded slow-wave high-power microwave (HPM) generator. *IEEE Trans. Plasma Sci.* **32**, 2236–2242.

https://doi.org/10.1017/S0263034613000633 Published online by Cambridge University Press